J. Fluid Mech. (2003), *vol.* 490, *pp.* 293–320.
DOI: 10.1017/S0022112003005366 Printed in the United Kingdom

Experimental measurements of the normal stresses in sheared Stokesian suspensions

By ANUGRAH SINGH† AND PRABHU R. NOTT‡

Department of Chemical Engineering, Indian Institute of Science, Bangalore 560 012, India

(Received 5 March 2002 and in revised form 21 April 2003)

We present experimental measurements of the normal stresses in sheared Stokesian suspensions. Though the suspending fluid is Newtonian, dispersing rigid non-Brownian particles in it yields a suspension that is non-Newtonian, as it exhibits normal stress differences and an excess isotropic pressure in viscometric flows. At small to moderate concentrations, the normal stresses are very small in magnitude, and hence difficult to measure. This difficulty is compounded by the presence of noise due to unavoidable experimental artifacts. Owing to these limitations, most measurements reported earlier were carried out at relatively high particle concentrations, and some at shear rates large enough that the effects of particle and fluid inertia may have been significant. In our study, we have used a novel technique to measure the small stress levels. This was achieved by applying a sinusoidally varying shear rate with a fixed (low) frequency superimposed on a constant shear rate, and using a lock-in amplifier to measure the Fourier component of the same frequency in the stress signal. We have measured normal stresses in cylindrical-Couette and parallel-plate geometries, and combined these measurements to determine the two normal stress differences for particle volume fractions in the range 0.3–0.45. While the normal stresses are very small at low concentrations, they rise rapidly with increasing concentration. The normal stresses vary linearly with the magnitude of the shear rate, and are independent of its sign. In contrast to polymeric solutions, both normal stress differences are negative, and the first normal stress difference is significantly smaller in magnitude. We compare our data with the results of earlier studies, and observe good agreement.

1. Introduction

The rheology of suspensions has been an intensely investigated subject over the past several decades. When the suspended particles are small enough, the inertia of the fluid and particles are unimportant in determining their dynamics. We refer to these systems as Stokesian suspensions, as the fluid motion is governed by the Stokes equations. Unless the particles are very small (typically, less than 1 μm), the effect of colloidal forces and Brownian motion can be discounted. In this regime, it has often been assumed that the rheological behaviour of the suspension is Newtonian, and consequently the main focus has been on determining its effective viscosity as a function of the concentration and size distribution of the suspended particles.

† Currently at the Department of Chemical Engineering, Technion, Haifa 3200, Israel.
‡ Author to whom correspondence should be addressed: prnott@chemeng.iisc.ernet.in

The stresses generated in a fluid in any viscometric flow, i.e. steady unidirectional shear flows, are the shear stress σ_{21} and the normal stresses σ_{11}, σ_{22} and σ_{33}. Here, the subscripts refer to the velocity (1), velocity gradient (2) and vorticity (3) directions. The normal stresses are customarily written in terms of their differences $N_1 \equiv \sigma_{11} - \sigma_{22}$ and $N_2 \equiv \sigma_{22} - \sigma_{33}$. If there are no forces other than hydrodynamic acting on the particles, we can see on dimensional grounds alone that the shear stress must exhibit a linear dependence on the magnitude of the shear rate in a Stokesian suspension. As a result, the shear viscosity is expected to be Newtonian. For Newtonian fluids in viscometric flows, N_1 and N_2 vanish.

The deviation from Newtonian behaviour of non-colloidal Stokesian suspensions was first shown by Bagnold (1954), who measured a radial normal stress that varied linearly with the shear rate in a cylindrical-Couette apparatus. Later Gadala-Maria (1979) measured the difference $N_1 - N_2$ using a rheometer. However, it is only recently that these non-Newtonian characteristics have been recognized as generic behaviour of non-colloidal suspensions, and some attention has been given to their microstructural origin (Brady & Morris 1997).

The study of normal stresses in particulate suspensions is important for the same reasons as it is in polymeric fluids, as many effects that arise in the processing of these materials, such as die-swell of extrudates, edge fracture and other instabilities, are due to normal stress differences. In addition, the phenomenon of shear-induced particle migration in suspensions is also closely related to normal stresses. This link was shown by Nott & Brady (1994), who also argued that normal stress differences can act to modulate particle migration so that it is not necessarily down a shear rate gradient. Morris & Boulay (1999) used a simple model for the normal stresses to explain the anomalous migration observed in experiments on parallel-plate and cone–plate devices. From a fundamental perspective, normal stresses in a non-colloidal Stokesian suspension are worthy of study because they are the most important non-Newtonian characteristic it exhibits; there are no elastic effects. Though shear thinning, another non-Newtonian effect, has been observed in some studies on suspensions, we show here that it not necessarily connected to the presence of normal stress differences.

In the absence of non-hydrodynamic particle interactions, the shear stress is linear in the shear rate, yielding a Newtonian shear viscosity. Normal stress differences can arise only if there is anisotropy in the microstructure. This is a result of the fore–aft symmetry of hydrodynamic forces on a sphere due to the motion of other spheres around it. If an anisotropic microstructure exists and it is independent of the magnitude of the shear rate $\dot{\gamma}$, normal stresses that are linear in $|\dot{\gamma}|$ result. This is in contrast to dilute polymer solutions, where the normal stresses are quadratic in the shear rate. Brady & Morris (1997) proposed a model in which a repulsive hard-sphere interaction breaks the fore–aft symmetry of the pair distribution in a dilute suspension, resulting in an anisotropic buildup of particles in the compression quadrant in simple shear that depends only on the sign the shear rate (but not its magnitude), and hence normal stresses that vary as $|\dot{\gamma}|$.

Investigations of the rheology and microstructure of Stokesian suspensions by computer simulation have proved to be effective, as artifacts that are normally unavoidable in experiments can be controlled with precision. The disadvantage of simulations is the large computational cost, limiting the system size to at most a few hundred particles. Phung, Brady & Bossis (1996) simulated the shear of Brownian suspensions, and reported that for large Péclet number (i.e. negligible Brownian motion) the first and second normal stress differences are of the same sign and comparable in magnitude. In our recent study (Singh & Nott 2000), the first normal

stress difference and the isotropic pressure were determined from simulations of bounded shear; to reduce computation time, particle motion was restricted to the velocity–velocity-gradient plane. More recently, Sierou & Brady (2001) conducted simulations of unbounded shear, without restricting the mobility of particles, and determined the two normal stress differences and the isotropic pressure. Both studies used a short-range repulsive interaction between the particles, and found a large enhancement of the pair distribution in a thin boundary layer near contact, as predicted by Brady & Morris (1997). However, their results do not show the scaling of the normal stresses with the range of the repulsive force that Brady & Morris predicted.

Experimental measurement of normal stresses in suspensions has been difficult to of their small magnitude and the prevalence of many troublesome artifacts. Bagnold (1954) was the first to report measurements of normal stresses, but most of his data were in the 'grain inertia' regime, where the stresses are induced mainly by particle collisions. In viscous flows, the intervening fluid prevents particle contact, and the stress arises purely from hydrodynamic particle interactions. Gadala-Maria (1979) measured $(N_1 - N_2)$ for the Stokes regime in the parallel-plate device of a rheometer, but encountered problems of poor repeatability and drainage of the suspension from the shear cell. Prasad & Kytoma (1995) measured the axial normal stress for highly concentrated suspensions (particle volume fraction ϕ in excess of 0.49) in a parallel-plate device. However, they equilibrated the fluid pressure with quiescent fluid across a perforated plate, thereby measuring only the stress arising from particle contacts, and not the viscous hydrodynamic stress. The most systematic study to date on normal stresses in Stokesian suspensions is that of Zarraga, Hill & Leighton (2000), who report data acquired by a combination of rheometry, surface profilometry, and re-interpretation of the viscous resuspension data of Acrivos, Mauri & Fan (1993). They used particles that were substantially heavier than the fluid, but argued that particle sedimentation was neutralized by shear-induced resuspension. There is a significant degree of scatter in their data, and deviation from linear dependence on the shear rate at high shear rates.

In this paper, we describe our experimental investigation to determine the normal stresses in suspensions. We have used a novel technique that is sensitive enough to measure the small stress levels, yet eliminate noise and errors from various sources. Most earlier studies have determined the normal stress differences using commercial rheometers, by measuring the total normal force on the stationary plate in parallel-plate and cone–plate devices. However, the lack of sensitivity of the force transducer makes the normal stress measurements prone to scatter and error. Initially, we too used a rheometer and obtained $N_1 - N_2$ from the total normal force in a parallel-plate device. However, we were unable to make reproducible measurements for particle volume fraction below 0.4, as the force was close to the instrument resolution. We then employed a sensitive technique that takes advantage of the linear dependence of the stress on the shear rate. In our experiments, the shear rate was modulated so that it varied sinusoidally about a constant baseline, with fixed frequency. To ensure that the relation between the stress and strain rate is as in any steady viscometric flow, the baseline shear rate was adjusted to keep the direction of shear constant (see § 3). The Fourier component of the signal from the stress transducer having the same frequency and phase as the shear rate was then measured, using a lock-in amplifier. This enabled the measurement of stresses as low as $1\,\mathrm{N\,m^{-2}}$, a head of roughly 0.1 mm of water. Experiments utilizing the above technique were conducted in cylindrical-Couette and parallel-plate geometries. The radial normal stress in the former and the

axial normal stress in the latter were measured for a range of particle concentration and shear rate. Combining the results for both the geometries, the two normal stress differences were determined. The scatter in our data is far lower than that of earlier studies.

In the following section, we describe our initial, unsuccessful, attempt to determine the normal differences using a commercial rheometer. The new technique we have devised to measure the small stress levels is described in § 3. The details of our experimental assembly and the materials used to make the neutrally buoyant suspension are given in § 4. The interpretation of our measurements to determine the material functions of interest is described in § 5, followed by the description of our results in § 6. Our main findings are then summarized and their implications discussed in § 7.

2. Preliminary experiments

Initially, we attempted to measure the normal stresses using a rheometer (TA Instruments). This instrument measures the total thrust $\mathscr{F}$ on the (stationary) lower plate. In the parallel-plate geometry, we can obtain one combination of normal stress differences from $\mathscr{F}$ using (Barnes, Hutton & Walters 1989)

$$N_1 - N_2 = \left(\frac{\mathscr{F}}{\pi R_o^2}\right)\left[2 + \frac{\mathrm{d}\ln\mathscr{F}}{\mathrm{d}\ln\dot{\gamma}_o}\right], \tag{2.1}$$

where R_o is the radius of the plates, and $\dot{\gamma}_o \equiv \dot{\gamma}(R_o)$ is the shear rate at the rim. The experiment can, in principle, also be conducted with the cone–plate geometry, but it is not usually used for particulate suspensions as there is a possibility of particles jamming in the gap near the apex of the cone. In these preliminary experiments, we used particles of 116 μm mean diameter and a fluid of the same density as the particles (see § 4). The gap H between plates was between 1 and 2 mm. The temperature was maintained at 20°C using the Peltier device coupled to the lower plate. The concentration of particles is quantified by the volume fraction ϕ. While the procedure is straightforward, we found it difficult to maintain the sample in the gap for a long period of time, as the gap was too large for the fluid to be held by surface tension.

When a sample of pure suspending fluid was loaded in the rheometer, its behaviour was found to be Newtonian, i.e. the viscosity remained independent of the shear rate, and the normal force on the lower plate was zero. Figure 1 shows the trace of the suspension viscosity η_s and the axial normal force $\mathscr{F}$ with time for a suspension with $\phi = 0.4$. Considering first the data for shear rate of $10\,\mathrm{s}^{-1}$, we see that both η_s and $\mathscr{F}$ reach steady values after a short time. The combination of normal stress differences $N_1 - N_2$ was computed using (2.1) from the measurement of $\mathscr{F}$, and the result is shown in figure 2. The linear dependence of $N_1 - N_2$ on the shear rate is evident, demonstrating that our measurements are indeed in the viscous regime.

At the higher shear rate of $30\,\mathrm{s}^{-1}$, however, figure 1 shows a continuous decrease of η_s, and a rise in $\mathscr{F}$, with time. At higher particle concentrations, the drift in η_s and $\mathscr{F}$ is more pronounced. At lower particle concentrations the normal force is small and, therefore, difficult to measure; there is considerable scatter and repeatability was difficult to achieve. Increasing the shear rate led to a rise in $\mathscr{F}$, but also in the drift. Though the drift can be minimized if the measurement is made in a short enough period of time, we were unable to make accurate and repeatable measurements of $\mathscr{F}$ within such a short period. The drift in η_s and $\mathscr{F}$ is most likely a result of drainage

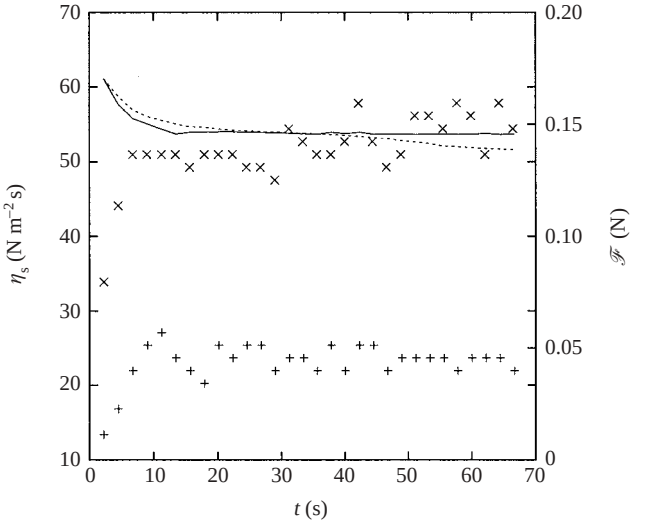

FIGURE 1. Time trace of the suspension viscosity η_s (lines) and the normal thrust $\mathscr{F}$ (symbols) during shear of a suspension in the parallel-plate device of our rheometer. The solid line and + are for a shear rate of $10\,\mathrm{s}^{-1}$; the dashed line and × are for $30\,\mathrm{s}^{-1}$. The volume fraction ϕ of particles is 0.4 and their mean diameter is 116 μm. Note the drift in the viscosity and normal force for the larger shear rate.

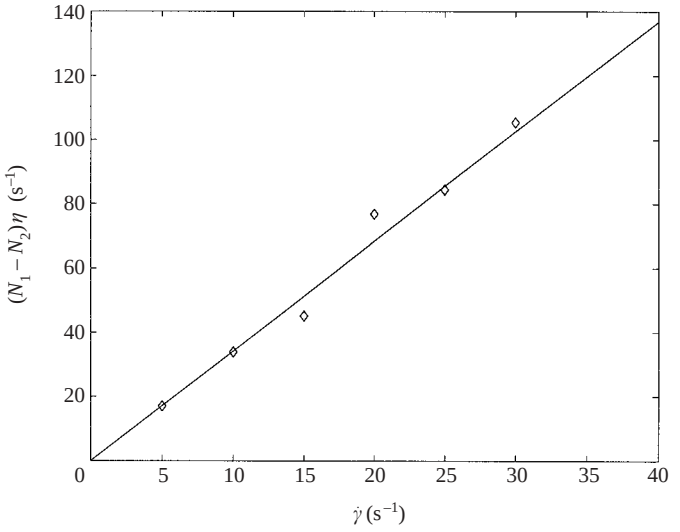

FIGURE 2. The combination of normal stress differences $N_1 - N_2$, scaled by the fluid viscosity η, determined from the thrust $\mathscr{F}$ on the parallel-plate device of our rheometer, using (2.1). The size and concentration of particles are as in figure 1. The straight line is a least-square fit through the data.

of suspension from the shear cell, but shear-induced particle migration may also play a role.

As a result of these difficulties, we were unable to make accurate and reproducible measurements of the normal stresses for a range of the particle concentration using a rheometer. This led us to design and construct an apparatus for the measurement of normal stresses in suspensions, which we describe below.

3. A new technique of measuring normal stresses

To avoid the above difficulties and minimize other instrumental artifacts, we devised a sensitive technique for measuring the normal stresses. In this method, rather than shear the suspension at a constant shear rate and measure the stress, we imposed a shear rate that varies sinusoidally in time with constant frequency. The component of the stress that is of the same frequency is then 'locked-onto', thus eliminating noise and errors that are not of the excitation frequency.

However, imposing a pure sinusoidal shear rate poses a problem: as the steady-state microstructure is fore–aft asymmetric (Parsi & Gadala-Maria 1987; Brady & Morris 1997), it will be disrupted during reversal of the shear direction twice in each cycle. This results in the stress having a different, more complicated, dependence on the shear rate than in steady viscometric flows. To overcome this, we superimpose a constant shear rate over the sinusoidally varying component, with its magnitude chosen so that the direction of shear is never reversed. This can be justified by the following consideration: the linearity of Stokes flow implies, as mentioned in § 1, that the normal stresses in a viscometric flow vary as

$$\sigma_{ii} = \eta\, \alpha_i\, |\dot{\gamma}|, \tag{3.1}$$

where η is the viscosity of the fluid, and the α_i are functions of the microstructure. Upon shearing, the α_i reach asymptotic values that do not depend on the the shear rate. Hence, they do not change when the shear rate is increased or decreased. However, they undergo a transient when $\dot{\gamma}$ changes sign, as a result of the microstructure having to readjust when the compression and tension axes are interchanged (Kolli, Pollauf & Gadala-Maria 2002). If we superimpose two shear rates $\dot{\gamma}_a$ and $\dot{\gamma}_b$ such that their sum never changes sign, the microstructure remains stationary in time, and the stress at any time depends only on the shear rate at that instant. In other words, the net stress is a linear superposition of the stresses due to the two shear rates. Thus, we can measure the material properties for steady shear by superimposing oscillatory and steady shear rates.

If the material response is nonlinear, superimposing a steady and oscillatory shear rate will not, in general, yield the material properties corresponding to steady shear – the net stress is not a linear combination of that due to the components of the shear rate. Further, an oscillating shear rate may induce a response different from that of steady shear. However, if the stress is linear in the imposed shear rate, the net stress is a linear superposition of that due to the components of the shear rate. Further, if there is no elasticity in the material response, the material properties for oscillatory shear rate will equal that for steady shear rate.

The following subsection describes the basic principle of lock-in measurements.

3.1. *Principle of lock-in measurements*

Lock-in amplifiers are used to measure small AC signals, even when they are drowned by noise many thousand times larger than the signal (Luppold 1969; Singh 2001). Typically the experiment is excited by an input (which in our case is the imposed shear rate) of a fixed reference frequency ω_{ref}, and the lock-in detects the response at the same frequency. In our measurements, the lock-in amplifier provided the reference signal, but an externally generated reference (using a function generator, for example) can also be used. When an external reference is used, the lock-in amplifier uses a phase-locked-loop (PLL) to lock its internal oscillator to the external reference.

Any signal can be represented as a Fourier sum of sine and cosine waves of different amplitudes and frequencies. In the lock-in amplifier, the signal to be measured is

multiplied by a pure sine wave of the reference frequency and averaged in time. Since sine waves of different frequencies are orthogonal, i.e. the time average of their product is zero, only the component of the signal with frequency ω_{ref} remains. Time averaging in the lock-in amplifier is accomplished by the low-pass filter, which follows the multiplier. This yields a DC output in proportion to the amplitude of the signal component of frequency ω_{ref}.

Consider an input signal $V_{\text{sig}} \sin(\omega_{\text{ref}} t + \theta_{\text{sig}}) + \mathscr{V}_{\text{noise}}$, where V_{sig} is the amplitude of the signal we wish to measure and $\mathscr{V}_{\text{noise}}$ is the noise we wish to filter. The lock-in amplifier first amplifies the signal with gain μ. Subsequently, its phase-sensitive detector (PSD) multiplies the signal by its internally generated reference $\mathscr{V}_\ell \equiv V_\ell \sin(\omega_\ell t + \theta_\ell)$, i.e.

$$\begin{aligned}\mathscr{V}_{\text{psd}} &= \mu V_{\text{sig}} V_\ell \sin(\omega_{\text{ref}} t + \theta_{\text{sig}}) \sin(\omega_\ell t + \theta_\ell) + \mu \mathscr{V}_{\text{noise}} \mathscr{V}_\ell \\ &= \tfrac{1}{2}\mu V_{\text{sig}} V_\ell \cos([\omega_{\text{ref}} - \omega_\ell]t + \theta_{\text{sig}} - \theta_\ell) \\ &\quad - \tfrac{1}{2}\mu V_{\text{sig}} V_\ell \cos([\omega_{\text{ref}} + \omega_\ell]t + \theta_{\text{sig}} + \theta_\ell) + \mu \mathscr{V}_{\text{noise}} \mathscr{V}_\ell. \end{aligned} \tag{3.2}$$

Thus the PSD output comprises AC signals of frequencies $(\omega_{\text{ref}} - \omega_\ell)$ and $(\omega_{\text{ref}} + \omega_\ell)$, and similarly, the sum of and difference between ω_ℓ and all the noise frequencies. If $\omega_\ell = \omega_{\text{ref}}$, the first term on the right-hand side of (3.2) is a constant. The other terms are AC signals, except in the unlikely case of the noise having a component whose frequency is exactly equal to ω_{ref}. This PSD output is then passed through a narrow-bandwidth low-pass filter to remove all AC components, yielding

$$V_{\text{out}} = \tfrac{1}{2}\mu V_{\text{sig}} V_\ell \cos(\theta_{\text{sig}} - \theta_\ell), \tag{3.3}$$

i.e. a pure DC output which is proportional to the signal amplitude V_{sig}.

The phase difference $\theta_{\text{sig}} - \theta_\ell$ is estimated by using a second PSD with a reference oscillator shifted by 90°, i.e. $V_\ell \sin(\omega_\ell t + \theta_\ell + 90°)$, which yields the output

$$V'_{\text{out}} = \tfrac{1}{2}\mu V_{\text{sig}} V_\ell \sin(\theta_{\text{sig}} - \theta_\ell). \tag{3.4}$$

Combining (3.3) and (3.4), we obtain the amplitude and phase of the input signal relative to the lock-in reference signal.

In our experiments the amplitude of the shear rate modulation was fixed and the amplitude of the normal stress measured by the lock-in amplifier. The phase difference between the stress and shear rate was found to be very small, never greater than 2°. The linearity in the relation between the stress and the shear rate allows us to use their respective amplitudes in (5.5) and (5.6) to calculate the material functions of interest.

When it is known *a priori* that the noise in the signal is of much higher frequency than the inverse of the measurement time, it is not necessary to use the frequency and phase-locked technique described above – the conventional method of using a low-pass filter is adequate. The lock-in technique is useful when components of the noise are of low frequency, such as the wobble of the rotor in our experiment (see § 5.2). The lock-in technique is inappropriate when an oscillatory driving force leads to unwanted dynamics; for instance, the response of a polymer solution to an oscillatory shear rate will differ from that in steady shear flow, as oscillations will excite the elasticity of the material. Lastly, the frequency of the driving force should not equal the frequency of an undesirable noise component. This is normally checked by varying the reference frequency over a range and verifying that the properties remain unchanged.

Most of our measurements were carried out using a very low reference frequency, usually 0.05 Hz, so that it is much lower than the noise frequencies arising from electronic manipulation of the signal. There was also enough separation between the reference frequency and the low-frequency noise due to mechanical sources, such as wobble in the inner cylinder (see § 5.2), for the lock-in to resolve and eliminate the latter. This was ascertained by trying a range of ω_{ref} (below 0.5 Hz), and ensuring that the stress remained insensitive to it.

4. Materials and method

The particles used in preparing the suspensions were poly (methylmethacrylate) spheres of density 1190 kg m^{-3} (Bangs Laboratories). Three batches, of mean diameter 116, 140 and 196 μm, were used. A suspending fluid of the same density as the particles was prepared using the recipe of Krishnan, Beimfohr & Leighton (1996), by mixing 71.12 weight % Triton X-100, 12.40% water and 16.48% anhydrous zinc chloride. The viscosity of the suspending fluid was found to be 2.19 N m^{-2} s at 25°C. The suspensions were prepared by mixing the appropriate amounts of particles and the suspending fluid in a beaker. Approximately 65 ml of suspension was required to fill the cylindrical-Couette apparatus, but considerably less for the parallel-plate apparatus. They were thoroughly mixed to achieve homogeneity and rested overnight to allow entrained air bubbles to rise, which were then skimmed off before loading the shear cell.

The two normal stress differences were determined by combining measurements of normal stresses in cylindrical-Couette and parallel-plate shear cells, which were fabricated specifically for this purpose. In the cylindrical-Couette device, the radial normal stress σ_{rr} was measured on the stationary outer cylinder roughly midway between the base and the free surface of the suspension, so as to avoid end effects. In the parallel-plate geometry, the axial normal stress σ_{zz} was measured on the stationary bottom plate at three radial positions. The three measurement ports were at the axis, and 1 cm and 2 cm from the axis. In both geometries, the stresses were measured once each for clockwise and counter-clockwise rotation of the motor.

The cylindrical-Couette cell (figure 3*a*) comprised an outer cylinder (cup) of inside diameter $2R_o = 55$ mm and an inner cylinder (rotor) of outside diameter $2R_i = 45$ mm, both 60 mm in height. To maintain a uniform shear rate throughout the gap, the bottom end of the rotor was a cone of angle 14°, truncated 5 mm from the apex. High-precision angular contact bearings in conjunction with flexible couplings ensured that the wobble of the rotor was not more than 10 μm at the base. The parallel-plate apparatus (figure 3*b*) consisted of a top plate of diameter $2R_o = 60$ mm rotating in a cup of diameter 100 mm. The gap H between the two plates was 4 mm. All components were constructed of stainless steel.

In the parallel-plate apparatus, the thickness of the sample to be tested is normally limited to a few hundred micrometres as the fluid is held between the plates by its surface tension. For a suspension, however, the gap should be greater than 10 times the particle diameter (i.e. a few millimetres) to prevent jamming. We found it difficult to maintain the sample in the gap for a long enough period of time without it draining out of the gap. To circumvent this difficulty, we used a rotating top plate over a pool of suspension (see figure 3*b*). While this may result in a departure from viscometric flow near the rim, its effect on normal stresses near the rotation axis is small (Bird, Armstrong & Hassager 1977, p 175). The only significant effect on the normal stresses within the shear cell due to the pool outside is that the outer rim is no

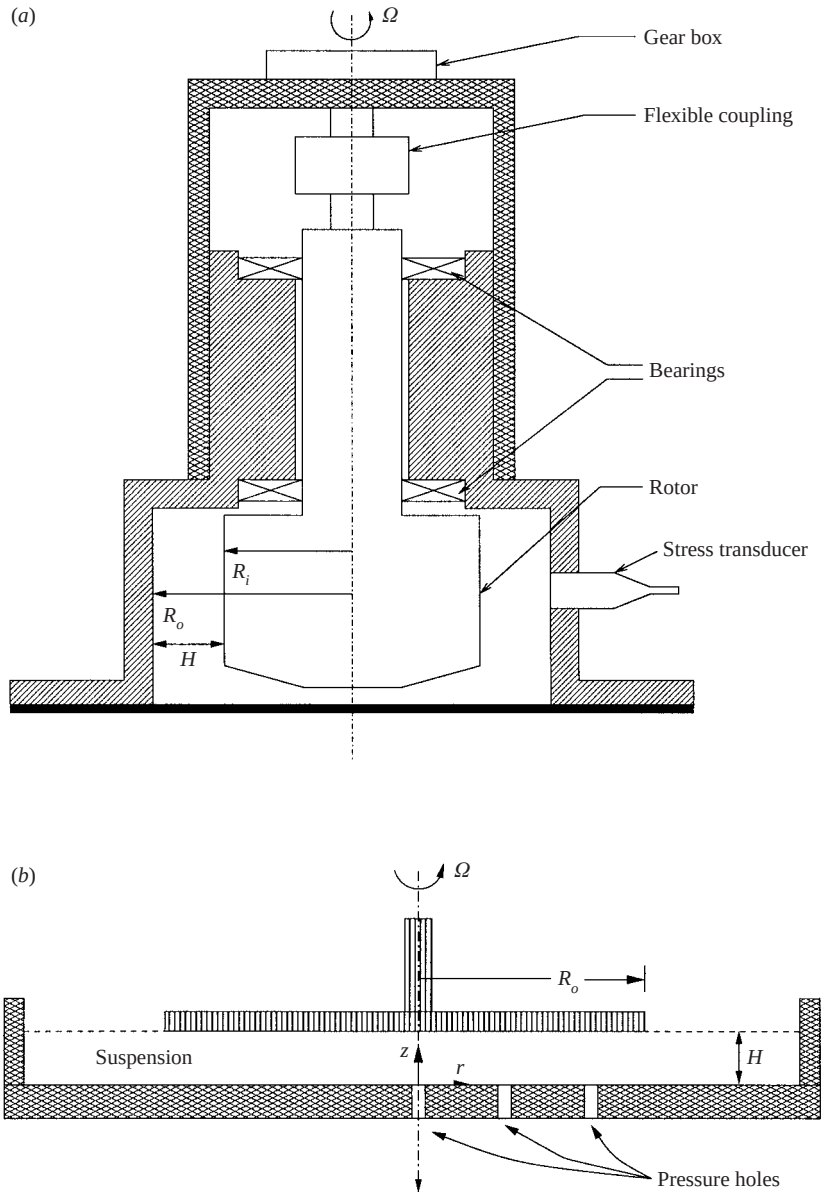

FIGURE 3. Schematic diagram of the cylindrical-Couette (*a*) and parallel-plate (*b*) devices used in this study. The drive train, bearings and housing for (*b*) are not shown, but are exactly as in (*a*).

longer at atmospheric pressure. This, however, leaves our measurements unaffected, as the lock-in amplifier measures only that component of the stress that is linear in the imposed shear rate (see § 5.1).

The rotation of the inner cylinder and top plate in the two experiments were driven by a precision DC servo motor (RS Controls). The motor was driven by a sinusoidal voltage at the reference frequency, provided by the lock-in amplifier, superimposed on a baseline DC voltage. The amplitude and frequency of the reference AC signal and the baseline DC voltage could be changed independently. The motor was controlled

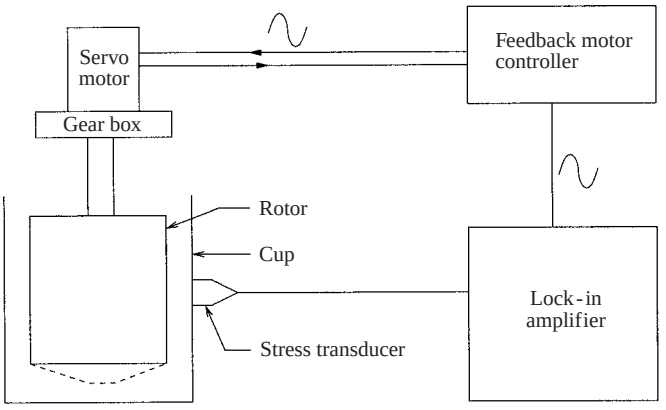

FIGURE 4. Schematic diagram of the experimental assembly. The lock-in amplifier provides an AC signal of frequency ω_{ref}, which, after amplification, is used to drive the motor. The lock-in amplifier captures only the component of the signal from the stress transducer that is of frequency ω_{ref}.

by a closed-loop feedback controller to achieve the prescribed sinusoidal variation of the speed; the controller adjusted the baseline DC voltage to correct deviations in the speed. A schematic diagram of our experimental assembly is given in figure 4.

The conventional method of measuring the normal stress at the bottom of a well drilled into the wall of the shear cell is not appropriate for suspensions, as particles will accumulate in the well as a result of shear-induced migration (Leighton & Acrivos 1987). We therefore used a flush-mounted stress transducer (Druck Ltd.) with a full scale of $700\,\text{N}\,\text{m}^{-2}$ and an active sensing area of 8 mm square. The transducer was fitted flush against the inner surface of the outer cylinder in cylindrical-Couette flow, and the lower plate in parallel-plate torsional flow, and sealed using silicone sealant. However, mounting a flat transducer perfectly flush against the curved surface of the cylinder is not possible. Moreover, the stress transducer was constructed in such a way that the active surface was recessed a fraction of a millimetre from its rim, and hence the mounting was also not perfectly flush in parallel-plate torsional flow. These factors introduced a small but systematic error in the stress, which is discussed in § 5.2.

The prepared suspension, after removal of air bubbles, was poured into the shear cell and the rotor was lowered into it. When the level of suspension stabilized, a sinusoidal rotation was applied to the rotor at the fixed reference frequency ω_{ref}. In most of our experiments ω_{ref} was set to 0.05 Hz, but we found the stress to be insensitive to the frequency as long as it was below 0.5 Hz. A sample time trace of the shear rate, determined from the speed signal from the motor, is shown in figure 5 along with the response from the stress transducer; the sinusoidal variation of both quantities is apparent, although the stress signal is noisy. After a few cycles, the lock-in amplifier locked on to the stress signal. The amplitude of the signal was recorded over the next 20 cycles and its time average noted. This procedure was repeated for five different amplitudes of the sinusoidal shear rate.

We also measured the normal stresses for pure fluids as a function of the viscosity in order to determine the 'hole pressure' error (see § 5.2). Low-molecular-weight silicone oils of different viscosities were used for this purpose.

For the system described above, the Reynolds number based on particle size, $\Re \equiv \rho\,\dot{\gamma} a^2/\eta$, was $O(10^{-3})$, and the Peclet number, $Pe \equiv \dot{\gamma} a^2/D_0$, was $O(10^{10})$ at a

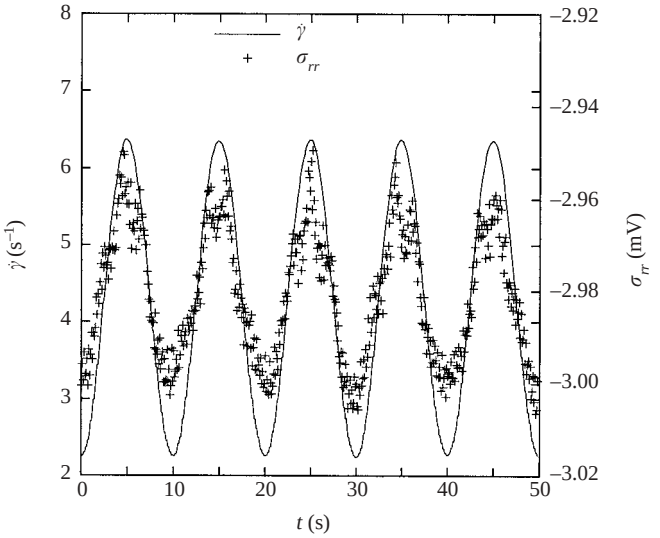

FIGURE 5. A typical sinusoidal profile of the shear rate, and the response from the stress transducer. The frequency of the shear rate, which is 0.1 Hz here, is set by the reference signal from the lock-in amplifier (see figure 4). Deviations from the desired shear rate profile are corrected by the feedback controller by adjusting the baseline DC voltage. Note the noise in the stress signal.

typical shear rate of operation. Here, ρ and η are respectively the density and viscosity of the suspending fluid, and a and D_0 are the radius and Brownian diffusivity of a suspended particle. Thus our measurements were well in the creeping flow regime with negligible Brownian motion. All our measurements were made in the temperature range 23–28°C.

At a reference frequency of 0.05 Hz, the time required for averaging the signal over 20 cycles is 400 s. This is much smaller than the time scale for shear-induced segregation of particles, which is estimated to be $\sim 10^5$ s for the cylindrical-Couette cell and even higher for the parallel-plate cell. We verified that there was no systematic change in the stress over the measurement time. Thus, all our measurements were on suspensions of uniform concentration.

5. Interpretation of data

As mentioned earlier, the normal stress differences N_1 and N_2 were determined by combining measurements of the radial normal stress σ_{rr} in cylindrical-Couette flow and the axial normal stress σ_{zz} in parallel-plate torsional flow. The lock-in amplifier measures only the stress generated by the shear rate component that oscillates with frequency ω_{ref}; the hydrostatic pressure is filtered out. In other words, the stress measured in our experiments is the dynamic (flow-induced) stress $\hat{\boldsymbol{\sigma}} \equiv \boldsymbol{\sigma} - p_{\mathrm{hyd}}\,\boldsymbol{I}$, where p_{hyd} is the hydrostatic pressure.

The material functions that characterize a suspension in steady viscometric flow are the shear viscosity η_s, and the first and second normal stress coefficients, defined as

$$\Upsilon_1 = -\frac{N_1}{|\dot{\gamma}|}, \quad \Upsilon_2 = -\frac{N_2}{|\dot{\gamma}|}. \tag{5.1}$$

The subscripts on the stress are as defined in § 1. Note that the above definitions of the normal stress coefficients differ from the conventional definition $\Psi_i = N_i/\dot{\gamma}^2$ used for polymeric fluids (Macosko 1994, p. 139). The normal stress differences in dilute polymer solutions are known to vary as $\dot{\gamma}^2$, but for Stokesian suspensions the linearity of Stokes flow dictates that the stress be a product of $\dot{\gamma}$ and a function of the microstructure. The anisotropy in the microstructure, which is responsible for normal stress differences (Brady & Morris 1997), depends only on the sign of $\dot{\gamma}$, and hence Υ_1 and Υ_2 as defined in (5.1) are independent of $\dot{\gamma}$. The sign of the normal stress coefficients in (5.1) is opposite to convention, because the normal stress differences in suspensions are negative (see figures 13 and 14).

As the suspension is incompressible, the reduced pressure $\Pi \equiv p/|\dot{\gamma}|$ is not a material property. The particle pressure as defined by Nott & Brady (1994) is for the particle phase, which is compressible – it is therefore legitimate to write a constitutive relation for this quantity. There is some ambiguity over the data for the pressure reported in previous studies; Zarraga *et al.* (2000) combined an estimate of the *particle-phase* normal stress in the vorticity direction (determined by applying the suspension balance model of Nott & Brady (1994) to the shear-induced re-suspension data of Acrivos *et al.* (1993)) with measurements of the normal stress differences for the *suspension* to derive the isotropic pressure. Singh & Nott (2000) and Sierou & Brady (2001), on the other hand, have determined Π for the suspension. We do not report our data for Π in this study as our data clearly show that it is not material property, but depends on the geometry of the shear cell; we leave the issue of resolving the differences in interpretation between previous measurements to a later study.

The rest of this section describes how the above material functions are determined from measurements of $\hat{\sigma}_{rr}$ in cylindrical-Couette flow and $\hat{\sigma}_{zz}$ in parallel-plate torsional flow.

5.1. *Theory*

Assuming that end effects are absent and that the particles are uniformly dispersed (so that the viscosity is independent of radial position), the velocity field in steady cylindrical-Couette flow is

$$u_\theta = \frac{\Omega\kappa^2}{(1-\kappa^2)}\left(\frac{R_o^2}{r} - r\right), \tag{5.2}$$

where r is the radial position, Ω is the angular velocity of the inner cylinder and $\kappa \equiv R_i/R_o$ is the ratio of the radii of the inner and outer cylinders. The shear rate at the outer cylinder, where the normal stress is measured, is then $\dot{\gamma}(R_o) = -2\Omega\kappa^2/(1-\kappa^2)$.

The axial normal stress σ_{zz} is simply given by the hydrostatic balance, i.e. $\sigma_{zz} = -p_{\mathrm{atm}} - \rho g h_s$, where h_s is the height of the suspension above the point of measurement. If h_s remains unchanged upon shearing the suspension, $\hat{\sigma}_{zz} = 0$ and the measured radial stress is therefore equal to the second normal stress difference, i.e. $N_2 = \hat{\sigma}_{rr}$. However, the presence of finite normal stress differences perturbs the free surface when the fluid is sheared; in polymer solutions, this is exemplified by the well-known Weissenberg (or 'rod-climbing') effect (Barnes *et al.* 1989) when a rotating rod is inserted into a bath of fluid. The normal stress differences are of opposite sign in Stokesian suspensions, and one therefore sees a depression of the free surface near the rotating rod (see the Appendix). This 'rod-dipping' phenomenon was first observed by Savage (1979), using a suspension of glass beads in bromoform. More recently, Zarraga *et al.* (2000) and Singh (2001) have observed the phenomenon using suspending fluids of much higher

viscosity (to ensure flow in the Stokes regime), and Zarraga *et al.* have estimated the normal stress differences by measuring the profile of the free surface.

As a result of the perturbation of the free surface, σ_{zz} is not just the hydrostatic head of the unsheared suspension, but reduced by $\rho g h(R_o)$, where $h(R_o)$ is the surface perturbation at the outer cylinder. It is determined by the normal stress differences N_1 and N_2, and is given by (see the Appendix)

$$\hat{\sigma}_{zz} = -\rho g h(R_o) = \alpha \left(N_2 + \tfrac{1}{2}N_1\right), \tag{5.3}$$

where α is a constant which depends only on κ. The second normal stress difference is therefore given by

$$N_2 = \hat{\sigma}_{rr} - \alpha \left(N_2 + \tfrac{1}{2}N_1\right). \tag{5.4}$$

Using (5.1), we can recast (5.4) in the form

$$(1-\alpha)\Upsilon_2 - \tfrac{1}{2}\alpha\Upsilon_1 = \frac{\hat{\sigma}_{rr}}{|\dot{\gamma}_o|}, \tag{5.5}$$

where $\dot{\gamma}_o \equiv \dot{\gamma}(R_o)$. This is the first equation for the determination of Υ_1 and Υ_2.

Note that the deflection of the free surface due to surface tension is independent of the shear rate, and hence leaves our measurement unaffected; we measure only the stress resulting from shear.

The second equation for determining Υ_1 and Υ_2 comes from our measurement of the axial normal stress $\hat{\sigma}_{zz}$ in parallel-plate torsional flow. We measure $\hat{\sigma}_{zz}$ as a function of r, the radial position from the axis of revolution, and determine $\hat{\sigma}_{zz}(r=0)$ by extrapolation (the normal stress at $r = 0$ cannot be measured directly because of the finite size of the stress transducer). This is repeated for different rotation speeds of the top plate, and the data thus obtained are related to the sum of the normal stress coefficients in the manner shown below.

Assuming that the flow is viscometric (i.e. negligible influence of the suspension pool outside the shear cell) the velocity field is $u_\theta = r\Omega z$ and the shear rate is $\dot{\gamma} = r\Omega/H$, where Ω is the angular speed of the upper plate (figure 3). Upon integrating the radial momentum balance from $r = 0$ to R_o, changing the integration variable to $\dot{\gamma}$, and differentiating the resulting equation with respect to $\dot{\gamma}_o$, we obtain the second equation for the determination of the normal stress coefficients

$$\frac{\mathrm{d}}{\mathrm{d}\dot{\gamma}_o}\left[\hat{\sigma}_{zz}(r=0)\right] = (\Upsilon_1 + \Upsilon_2)\,. \tag{5.6}$$

A complete derivation of (5.6) is given by Bird *et al.* (1977, pp. 177–178)†. The left-hand side is determined by measuring $\hat{\sigma}_{zz}$ at the axis of rotation for a range of the rotation rate Ω, and determining the slope.

Equations (5.5) and (5.6) determine the normal stress coefficients from independent measurements of the normal stresses in cylindrical-Couette and parallel-plate geometries.

Another method of determining the second normal stress coefficient Υ_2 is from the axial normal stress at the rim:

$$-\Upsilon_2\dot{\gamma}_o = \hat{\sigma}_{zz}(R_o) - \hat{\sigma}_{rr}(R_o) = \hat{\sigma}_{zz}(R_o), \tag{5.7}$$

† The slight difference between (5.6) and their relation arises from the difference in definitions of our normal stress coefficients Υ_i and their Ψ_i.

and hence

$$\Upsilon_2 = -\frac{\mathrm{d}}{\mathrm{d}\dot{\gamma}_o}(\hat{\sigma}_{zz}(R_o)). \tag{5.8}$$

However, measurement of the axial normal stress at the rim is susceptible to greater error than at the axis (see § 6.2). We therefore eschew the use of (5.8) to determine Υ_2, and use (5.5) and (5.6) instead, as described above.

Thus, combining measurements of the radial normal stress in cylindrical-Couette flow and the axial normal stress in parallel-plate torsional flow with the estimate of the free-surface perturbation in cylindrical-Couette flow allows us to determine the two material functions Υ_1 and Υ_2.

5.2. *Measurement error*

Several sources of error complicate the measurement of stress, particularly if the latter is small in magnitude. One is the electronic noise that inevitably accompanies measurement and amplification of small signals; by using a lock-in amplifier we were able to ensure this was a very small fraction of the signal. The mechanical sources of error in our measurement were:

(*a*) axis of rotation eccentric and/or not parallel to the cylinder axis (wobble);
(*b*) axial movement of the rotating member;
(*c*) stresses due to fluid inertia and secondary flows;
(*d*) nonlinear material response;
(*e*) finite size of holes used for pressure measurement.

Among these, (*a*) and (*b*) can give rise to large oscillatory stresses, but they are filtered by the lock-in amplifier if the rotation frequency differs from the frequency of the applied shear rate.

Turning to source (*c*), the instability of steady unidirectional cylindrical-Couette flow first occurs by the formation of Taylor vortices when the Taylor number exceeds a critical value (Chandrasekhar 1961, p. 304):

$$Ta \equiv \frac{4\rho^2\Omega^2 R_i^4 R_o^4}{\eta^2\left(R_o^2 - R_i^2\right)^2} > Ta_c \approx 3400. \tag{5.9}$$

In our experiments Ta never exceeded 13, ruling out the influence of secondary flows.

Inertial effects may be present even in the absence of secondary flows; for instance, fluid inertia causes a concave free surface in cylindrical-Couette flow, resulting in an additional head at the outer cylinder

$$\sigma_{zz}^{\text{inertia}} = -\tfrac{3}{2}\rho\Omega^2 H^2. \tag{5.10}$$

We find $\sigma_{zz}^{\text{inertia}}/\eta\dot{\gamma}$ to be at most 0.05, which is far smaller that the viscous stresses we measured. In a parallel-plate device, fluid inertia tends to pull the plates together with a stress given by (Macosko 1994, p. 210)

$$\sigma_{zz}^{\text{inertia}} = 0.15\rho\Omega^2\left(r^2 - R_o^2\right). \tag{5.11}$$

For our parallel-plate experiments, $\sigma_{zz}^{\text{inertia}}/\eta\dot{\gamma}$ was never greater than 9×10^{-3}, which is again much lower than the viscous stresses we measured (figure 11).

If the shear rate were purely oscillatory, say $\dot{\gamma}_o \sin(\omega_{\text{ref}}\, t)$, the inertial stress would be proportional to $A^2/2(1 + \sin(2\omega_{\text{ref}}\, t - \pi/2)$. Hence it would be filtered out if the lock-in amplifier were locked to frequency ω_{ref}. However, since we superimpose a steady shear rate $\dot{\gamma}_s$ the inertial stress will have a component of frequency ω_{ref}

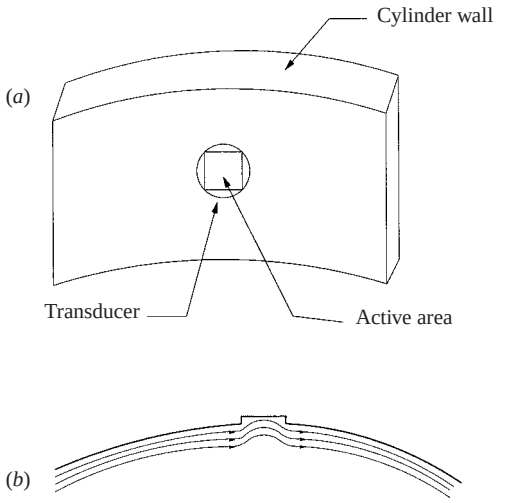

FIGURE 6. (*a*) The port on the outer cylinder of the cylindrical-Couette device, where the stress transducer is mounted. Mounting a flat transducer face on a cylindrical surface causes a depression, or hole, resulting in curvature of the fluid streamlines, shown in (*b*). A hole is also present in the parallel-plate device, because the active surface of the transducer is recessed slightly from its rim.

equal to $2\dot{\gamma}_s\dot{\gamma}_o \sin(\omega_{\text{ref}}\, t)$. It is therefore essential that the inertial stresses be small in comparison with the viscous stresses.

The above error also occurs if the material response is nonlinear (source (*d*)), unless *a priori* knowledge of the nonlinearity is available to enable correct interpretation of the measurement. In our experiments, the response was linear for the range of shear rate and concentration explored (see figures 8 and 9), and we therefore do not expect our measurements to be affected by this error. The nonlinearity of the response may be estimated by determining the higher harmonic components of the stress response, i.e. the components of frequency $2\,\omega_{\text{ref}}$, $3\,\omega_{\text{ref}}$ etc., using the lock-in amplifier. We determined the second harmonic in one experimental run and found it to be negligibly small.

Source (*e*) is a common error which needs careful attention. It is not possible to mount a flat transducer surface flush against the curved surface of the outer cylinder; the transducer surface is either depressed or elevated with respect to the cylinder at its periphery (see figure 6*a*), resulting in deviation of the streamlines from circular. Further, a secondary flow is caused at the periphery of the transducer surface. This leads to the well-known 'hole pressure error' (Macosko 1994, p. 262; Bird *et al.* 1997, p. 97), a pressure in excess of the hydrostatic even for a pure fluid. This effect is also present in the parallel-plate device, because the active surface of the transducer is not perfectly flush with the lower plate but is recessed a fraction of a millimetre from it. As the Reynolds number is small, the hole pressure is also linear in the shear rate, and therefore cannot be filtered by the lock-in amplifier.

This difficulty was overcome by measuring the hole pressure for Newtonian fluids, which was then used to correct the normal stress measurements for suspensions. To this end, the hole pressure p_h was determined during shear of low-molecular-weight silicone oils of different viscosity. The hole pressure varies linearly with the shear rate, as shown in figure 7(*a*). From these data the calibration curve for $p_h/\dot{\gamma}$ was determined as a function of the viscosity of the silicone oil, which is shown in figure 7(*b*). In the

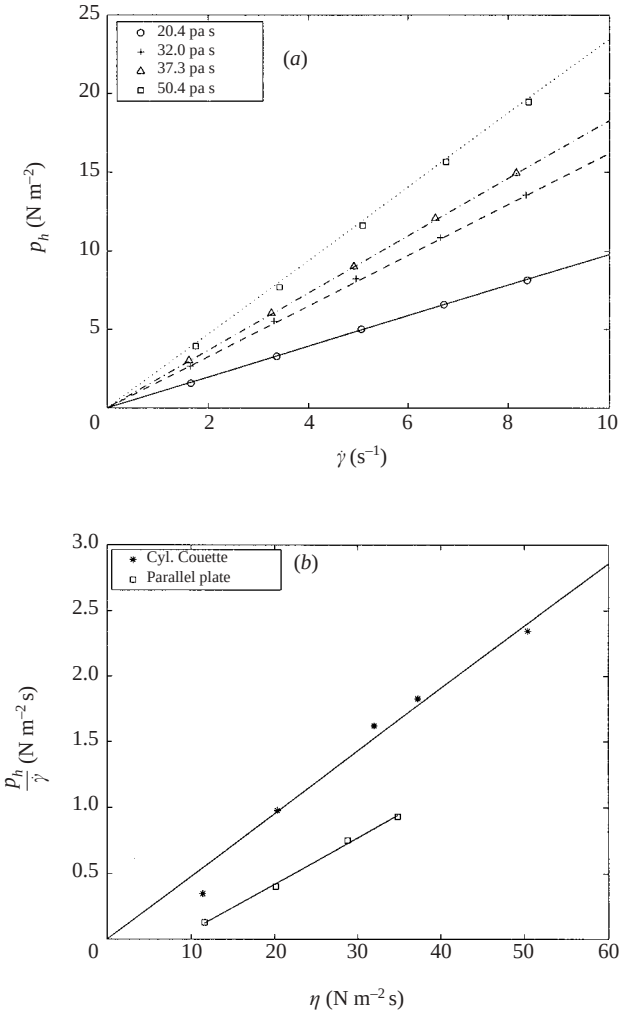

FIGURE 7. (*a*) The hole pressure p_h as a function of the shear rate for silicone oils of different viscosities in the cylindrical-Couette device. Linear dependence of p_h on $\dot{\gamma}$ is observed here and in the parallel-plate device (not shown). (*b*) The calibration for $p_h/\dot{\gamma}$ as a function of fluid viscosity, which is used to correct the normal stress measured in a suspension. The parallel-plate data are for the central pressure port.

parallel-plate device, the hole pressure turns negative (tensile) for low fluid viscosity. Though this could be a result of inertial effects becoming significant at low viscosity, we observed the hole pressure to vary linearly with the shear rate; we therefore do not understand the reason for the change in sign of p_h. The normal stress measured in a sheared suspension of known effective viscosity was scaled by the shear rate and the value of $p_h/\dot{\gamma}$ at that viscosity (determined from figure 7*b*) was subtracted from it. The resulting stress is only due to the presence of particles, and is hence a true measure of the particle stress.

The procedure described above assumes that the hole pressure error arises entirely from the secondary flow in the recessed volume. It is however well-known that the normal stress differences themselves can yield a hole pressure (Bird *et al.* 1977, p. 97), hence it is necessary to assess its influence in our experiments. This effect is felt

when there is a deep hole or well, at the base of which is the pressure sensing surface. Assuming that the shear stress drops to zero at the pressure-sensing surface, one can determine the pressure error due to the curvature of the streamlines across the hole (Bird *et al.* 1977, pp. 99–101). In our experiment, however, the depth of the hole is a small fraction of its diameter, roughly 1/20. Hence the curvature of the streamlines would have been negligibly small, and the shear stress at the sensing surface would have deviated very little from the value at the wall. Therefore, we expect that the influence of the normal stress differences on the hole pressure to have been insignificant.

6. Results

6.1. *Suspension viscosity*

The shear viscosity of the suspension is required to determine the hole pressure contribution to the normal stress. The viscosity was measured using a cylindrical-Couette cell in a Haake viscometer, at the same temperature at which the normal stress measurements were made. Figure 8(*a*) shows that there is some shear thinning for $\phi = 0.5$, but that it is absent for smaller concentrations. Zarraga *et al.* (2000) also observed shear thinning, and found the shear stress to obey a power law $\tau \sim \dot{\gamma}^n$, with n decreasing from 0.99 to 0.8 as ϕ increased from 0.3 to 0.55. Though the phenomenon of shear thinning in non-colloidal suspensions is well known (Leighton 1985), a good explanation for it is lacking. In our study, we have side-stepped the issue of shear thinning by conducting experiments in the regime of shear rate and particle concentration where shear thinning is absent. Figure 8(*b*) shows our data for the relative viscosity η_r (suspension viscosity scaled by the fluid viscosity) as a function of the particle concentration, along with the data of Zarraga *et al.* (2000). Both sets of data agree well with the Eiler fit (Leighton 1985; Zarraga *et al.* 2000),

$$\eta_r(\phi) \equiv \eta_s/\eta = \left(1 + \frac{1.5\phi}{(1-\phi/\phi_p)}\right)^2, \tag{6.1}$$

with $\phi_p = 0.58$.

6.2. *Normal stresses*

Unless stated otherwise, all our data were obtained using particles of mean diameter of 196 μm. Figure 9 shows the normal stresses as a function of the shear rate for the two geometries. The measurements for clockwise and counter-clockwise rotation demonstrate linear dependence of the normal stress on $|\dot{\gamma}|$; they also show that the stress arises purely from viscous hydrodynamics. While $\hat{\sigma}_{rr}$ is negative, or compressive, in the cylindrical-Couette (figure 9*a*), $\hat{\sigma}_{zz}$ at the central port in the parallel-plate is tensile (figure 9*b*). The hole pressure is compressive in both geometries. At lower particle concentration, where the suspension viscosity is lower, the hole pressure error in the parallel-plate geometry is small but tensile (see figure 7).

The variation of the axial normal stress with radial position r for parallel-plate flow is shown in figure 10. The linear variation of $\hat{\sigma}_{zz}$ with r is apparent. Further, $\hat{\sigma}_{zz}$ changes sign beyond a certain r and becomes compressive. These observations can easily be understood if we consider the radial momentum balance, integrated from r to R_o:

$$\frac{H}{\Omega}\hat{\sigma}_{zz}(r) = (\Upsilon_1 + \Upsilon_2)(R_o - r) - \Upsilon_2 r. \tag{6.2}$$

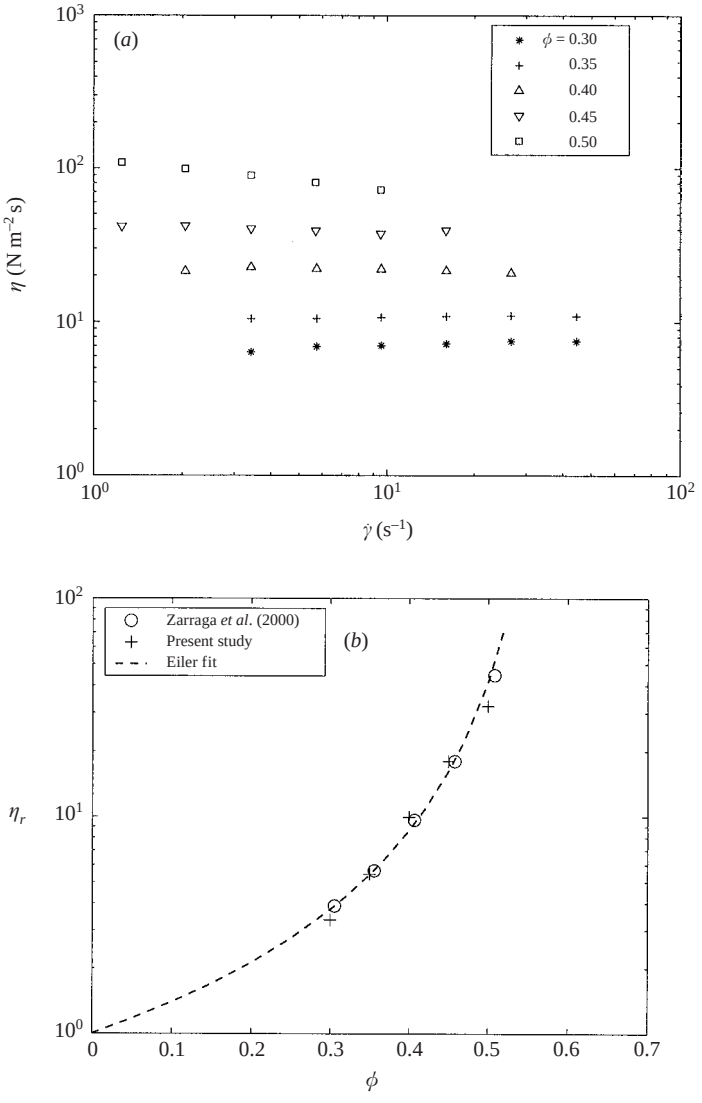

FIGURE 8. (*a*) Viscosity of the suspension as a function of the shear rate. (*b*) Relative viscosity as a function of the particle concentration ϕ.

It is now clear that $\hat{\sigma}_{zz}(r)$ varies linearly with r and, if Υ_1 and Υ_2 are of the same sign, it changes sign at a value of r greater than $R_o/2$.

A point to be noted regarding our measurement is that the transducer senses the pressure over a square of size 8 mm. The linear dependence of $\hat{\sigma}_{zz}$ on r then suggests that the stress measured at the central port should be assigned not to the centre, but to a distance from the centre equal to a quarter of the length of the sensing area, i.e. $r = 2$ mm. The positions assigned to the stresses at other two ports remain unaltered from their geometric centres. The normal stress at the axis is determined from the intercept of the lines in figure 10. The error due to extrapolation is quite small at the axis due its proximity to the data point at $r = 2$ mm. However, the error in estimating $\hat{\sigma}_{zz}$ at the rim ($r = 30$ mm) is much larger because of its distance from the measurement ports: a small error in estimating the slope of the line can result in

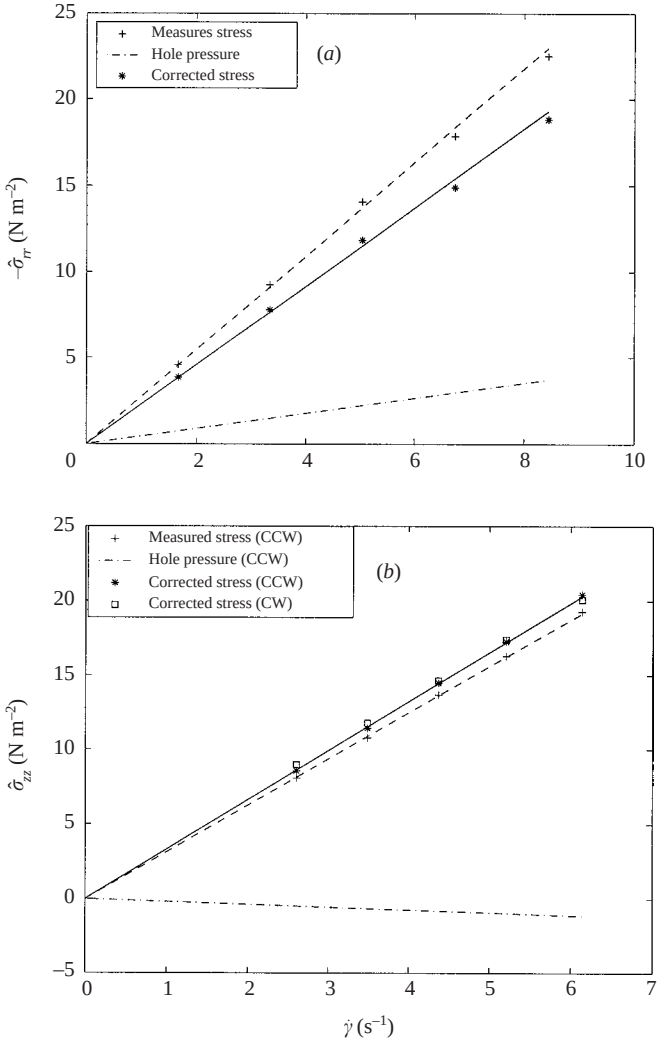

FIGURE 9. The radial normal stress $\hat{\sigma}_{rr}$ in cylindrical-Couette flow (a) and the axial normal stress $\hat{\sigma}_{zz}$ at the central port in parallel-plate flow (b) as a function of the shear rate. The mean diameter of the particles is 196 μm and $\phi = 0.35$. In (b), CW and CCW denote measurements made with clockwise and counter-clockwise rotations, respectively, of the rotor. The hole pressure is determined by shearing pure Newtonian liquids of various viscosities, as described in § 5.2.

a large error in the stress at the rim. It is for this reason that we do not determine the second normal stress difference from $\sigma_{zz}(R_o)$ using (5.8), but determine if from the normal stress at the axis using (5.6), as mentioned in § 5.1.

The procedure used to generate the data in figures 9 and 10 was repeated for other particle volume fractions in the range of 0.30–0.45. For volume fractions below 0.3, the signal was too small compared to the noise, and measurement repeatability was unsatisfactory; we therefore do not report these data. The normal stresses are shown in figure 11 as a function of ϕ. The normal stresses increase rapidly with ϕ, in accord with the results of our Stokesian Dynamics simulations (Singh & Nott 2000) and those of Sierou & Brady (2001).

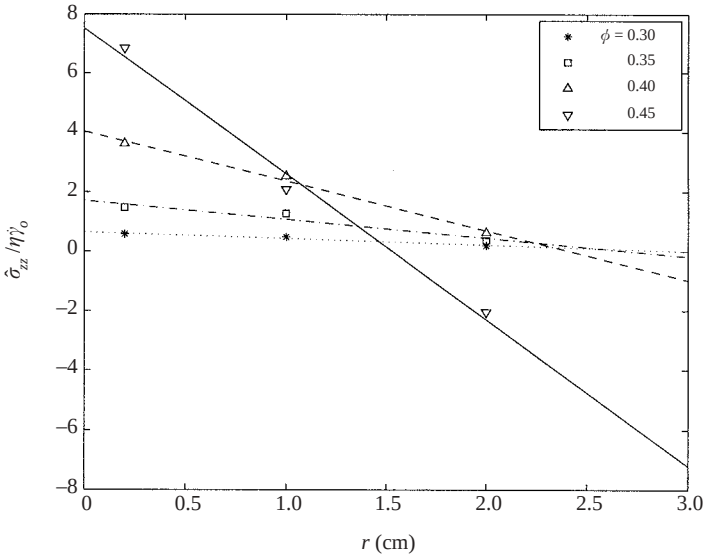

FIGURE 10. The axial normal stress $\hat{\sigma}_{zz}$ at different radial positions in the parallel-plate device. Here $\dot{\gamma}_o$ is the shear rate at the rim.

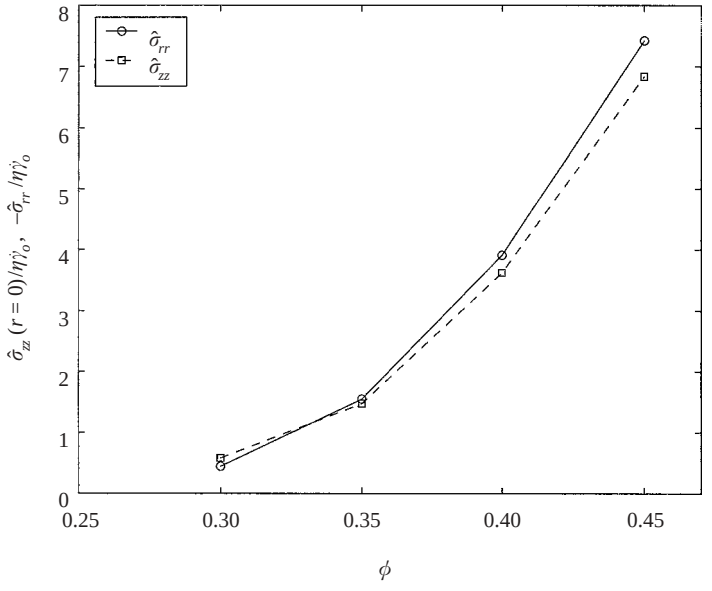

FIGURE 11. The normal stresses $\hat{\sigma}_{rr}$ (cylindrical-Couette) and $\hat{\sigma}_{zz}$ (parallel-plate) as a function of particle concentration.

To investigate the effect of particle size, we determined $\hat{\sigma}_{rr}$ in cylindrical-Couette flow for three samples of suspension made with particles of mean diameter 116, 140 and 196 μm. Our data (figure 12) reveal that the normal stresses are largely independent of the particle size. There appears to be a systematic rise in the stress with increasing particle diameter, probably a finite size effect which will vanish at large Couette gap, but the difference for the three sizes is clearly quite small.

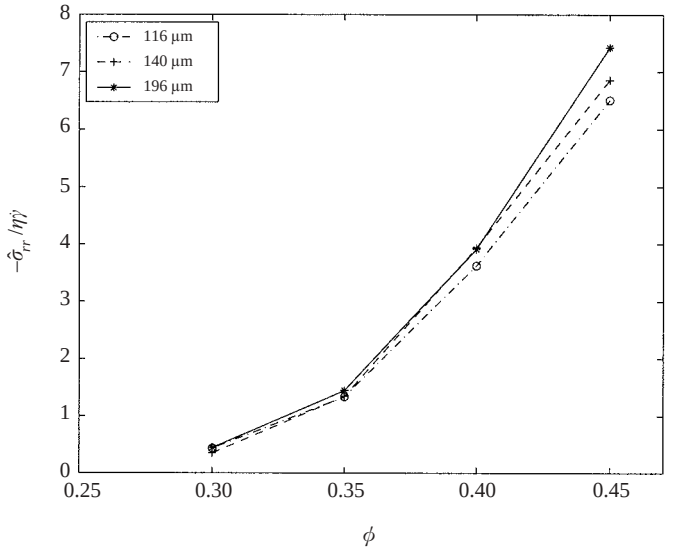

FIGURE 12. The radial normal stress $\hat{\sigma}_{rr}$ in cylindrical-Couette flow as a function of particle concentration for particles of three different sizes.

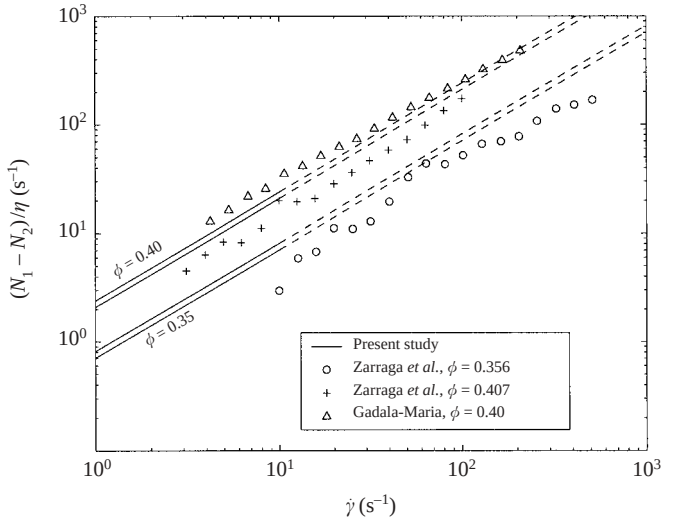

FIGURE 13. The combination $N_1 - N_2$ of the normal stress differences as a function of the shear rate. The two straight lines for each concentration are the two standard deviation error bounds of our measurements. The dashes indicate extrapolation to shear rates higher than our range of measurement. The data of Zarraga *et al.* (2000) are for their KG based suspensions.

The data in figure 11 can now be used to determine the material functions Υ_1 and Υ_2 using (5.5) and (5.6). We first consider the combination $N_1 - N_2 \equiv -(\Upsilon_1 - \Upsilon_2)\,|\dot{\gamma}|$, shown in figure 13, for the purpose of comparison with the data of Zarraga *et al.* (2000) and Gadala-Maria (1979). Both studies determined this combination of the normal stresses from measurements of the total thrust on the stationary bottom plate of a parallel-plate device using a rheometer (described in § 2). As our data come from a combination of measurements of normal stresses in the cylindrical-Couette and

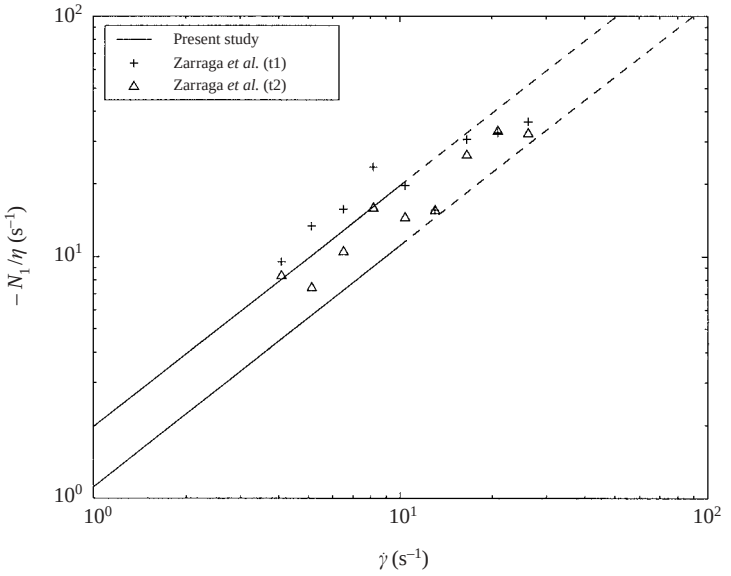

FIGURE 14. First normal stress difference N_1 as a function of shear rate for 45% PMMA suspension. The straight lines represent two standard deviation error bounds of data. The dashes indicate extrapolation to shear rates higher than our range of measurement. The symbols are data of Zarraga *et al.* (2000) for their "trial 1" (+) and "trial 2" (△) experiments with $\phi = 0.457$.

parallel-plate devices, which were not necessarily at the same shear rates, we cannot present our data points in this plot. The pair of lines for each concentration give the two standard deviation error bounds of the normal stresses versus the shear rate, determined from plots such as figure 9. (A short discussion on error estimates is given at the end of this section.) The scatter in our data is considerably lower, especially at the lower concentration, but there is reasonable overall agreement among all three sets of data.

Figure 14 compares our data for the first normal stress difference with that of Zarraga *et al.* (2000), and here we see good agreement. Here too, the lines represent two standard deviation error estimates of our data. The results of Zarraga *et al.* shown here are from their measurements of the total thrust in the cone–plate device of a rheometer. They also determined N_1 by another method, combining measurements of $N_1 - N_2$ in a parallel-plate device and $N_2 + N_1/2$ from the deflection in the free surface using surface profilometry; this procedure gave substantially lower values of N_1, as shown in figure 15.

It is evident from figures 13 and 14 that our technique has allowed the measurement of normal stresses for much lower shear rates than in the studies of Gadala-Maria and Zarraga *et al.*; this has limited experimental errors and artifacts, and reduced (or even eliminated) the influence of unwanted phenomena such as inertial effects and edge fracture.

The variation of the material functions Υ_1 and Υ_2 with particle concentration are tabulated in table 1 and displayed in figures 15 and 16. Also shown in the figures are the data of Zarraga *et al.* (2000), and the results of Stokesian Dynamics simulations of Singh & Nott (2000) and Sierou & Brady (2001). To make an appropriate comparison with the two-dimensional simulations of Singh & Nott (2000), their area fractions

ϕ	η	η_r	Υ_1/η (s_{Υ_1})	Υ_2/η (s_{Υ_2})
0.30	1.975	3.36	0.314 (0.0015)	0.314 (0.015)
0.35	2.06	5.44	0.4754 (0.0005)	1.23 (0.02)
0.40	2.06	9.94	0.900 (0.0074)	3.14 (0.04)
0.45	2.145	17.98	1.54 (0.083)	5.98 (0.20)

TABLE 1. Steady-shear material functions as a function of particle concentration. The fluid viscosity η is in $\mathrm{N\,m^{-2}\,s}$, and all other quantities are dimensionless. The quantities within parentheses in columns 4 and 5 are standard deviations.

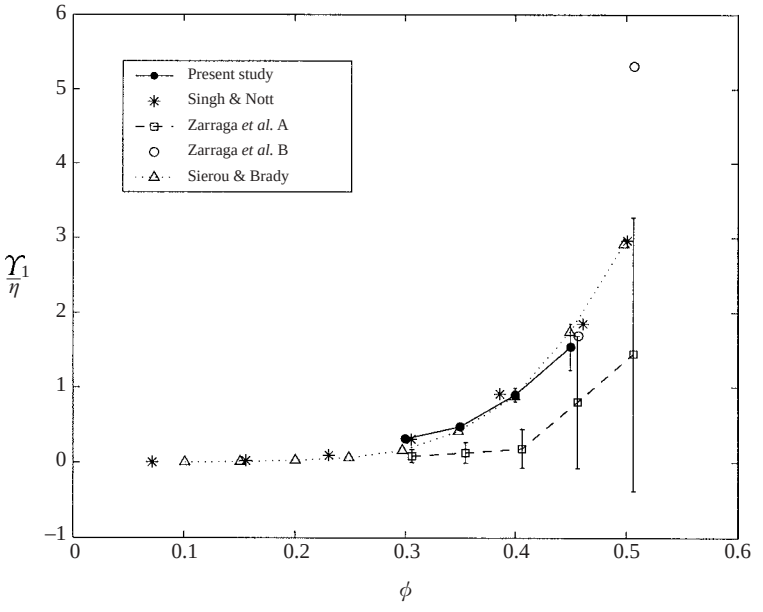

FIGURE 15. The first normal stress coefficient as a function of particle concentration. Also shown are experimental data of Zarraga *et al.* (2000) (A and B refer to their parallel-plate and cone–plate measurements, respectively) and simulation results of Singh & Nott (2000) and Sierou & Brady (2001). The area fractions of Singh & Nott are converted to volume fractions (see text) in order to make an appropriate comparison.

are converted to volume fractions by multiplying by the ratio of maximum random packing volume fraction in three and two dimensions, $\phi^{3d}_{\max}/\phi^{2d}_{\max}$. Our data for Υ_1 are in good agreement with the simulation results, but the data of Zarraga *et al.* (squares) are considerably lower and their errors much larger. Their measurements of Υ_1 using the cone–plate device (circles) are much closer to our data and that of the simulations, but they were unable to make measurements for $\phi < 0.457$ as they found the signal "small and hard to measure" in this geometry. There is reasonable agreement between their data for Υ_2 and ours in figure 16, but the simulations of Sierou & Brady predict significantly lower values of this material function. Singh & Nott could not determine Υ_2 from their monolayer simulations. Thus, Υ_2 is found to be roughly four times larger than Υ_1 in the experiments, while the simulations of Sierou & Brady find them to be of roughly equal magnitude. The latter authors have speculated that the reason

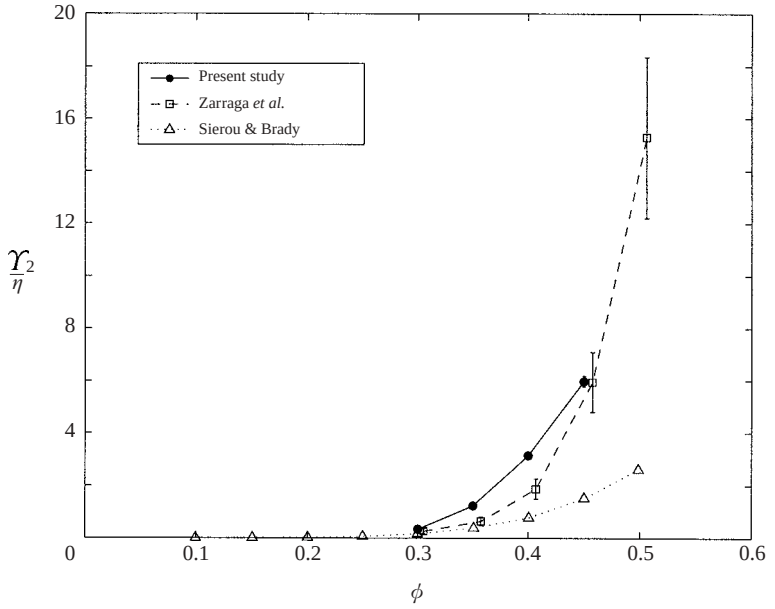

FIGURE 16. The second normal stress coefficient as a function of particle concentration. Also shown are experimental data of Zarraga *et al.* (2000) and simulation results of Sierou & Brady (2001).

for this discrepancy is the presence of frictional particle contacts, which are not allowed in Stokesian Dynamics simulations. While this is a possibility, we believe that the inter-particle repulsive force used in the simulations is a more likely cause of the discrepancy; the repulsive interaction plays a significant role in determining the anisotropic microstructure (Singh & Nott 2000; Sierou & Brady 2001), and thereby the normal stress differences. We comment further on this point in the concluding section.

As mentioned above, the lines in figures 13 and 14, and error bars in figures 15 and 16 represent two standard deviation envelopes of the scatter in our data. We determined the standard deviation by estimating the variance of the slope (Cochran 1967) of the normal stress versus shear rate, in plots such as figure 9. The error bars for our data in figures 15 and 16 are generally quite small, in most cases smaller that the size of the symbols used for the data points. They were determined from the standard deviations of the two independent measurements† (see (5.5) and (5.6)), assuming that the errors in the two are uncorrelated (Cochran 1967). The error bars for the data of Zarraga *et al.* (2000) in figures 15 and 16 were determined similarly, from the errors for $N_1 - N_2$ and $N_2 + 1/2N_1$ reported in their paper. Sierou & Brady (2001) determined the statistical variation of properties by dividing a simulation run into subintervals, and using the properties in each as an independent measurement. They found that the variation for all rheological properties was usually less than 5%, and we therefore do not report them here. Singh & Nott (2000) did not analyse their simulation results to determine the temporal variation of properties.

† For a quantity $z = ax + by$ derived from measurements of x and y, whose respective standard deviations are s_x and s_y, the standard deviation s_z is given by $s_z^2 = a^2 s_x^2 + b^2 s_y^2$.

7. Summary and conclusions

We have experimentally determined the normal stresses differences in non-Brownian Stokesian suspensions from direct measurements of the normal stresses in cylindrical-Couette and parallel-plate devices. The suspensions studied were neutrally buoyant, i.e. the densities of the particles and fluid were closely matched, so as to avoid gravitational settling of the particles.

Using a novel and sensitive technique that takes advantage of the linear response of Stokesian suspensions, we were able to measure normal stresses as low as $1\,\mathrm{N\,m^{-2}}$. Rather than shear the suspension at constant shear rate, as is the normal procedure in rheological experiments, a shear rate that varied sinusoidally in time with a fixed reference frequency ω_{ref} was superimposed on the constant shear rate. The amplitudes of the constant and oscillating components were adjusted so that the net shear rate never changed sign, to ensure that the microstructure remained stationary in time. The component of the signal from the stress transducer with frequency precisely ω_{ref} was then extracted using a lock-in amplifier. This technique filters the mechanical and electronic noise and errors from other experimental artifacts that are inevitably present in the measurement of small stresses, thereby allowing accurate and repeatable measurement of the normal stresses. Using this technique we have measured the normal stresses at shear rates far lower, and measurement accuracy significantly higher, than in earlier studies (Zarraga *et al.* 2000; Gadala-Maria 1979). We have reported measurements for particle volume fraction ϕ in the range 0.3–0.45; the normal stresses for $\phi < 0.3$ were too small and could not be measured accurately even by this technique.

In the regime of particle concentration and shear rate that we have considered, the shear viscosity of the suspension is Newtonian, i.e. it is independent of the shear rate. The normal stresses vary linearly with the magnitude of the shear rate $|\dot{\gamma}|$, but do not change sign upon reversal of the direction of shear. This interesting result shows that a sheared Stokesian suspension is fundamentally far from equilibrium; a small perturbation about equilibrium would have resulted in the normal stresses varying as $\dot{\gamma}^2$, as in dilute polymer solutions. This behaviour can be understood if we recognize the relation between the microstructure of the suspension and its rheology: for a given distribution of particles, the linearity of Stokes flow implies that the normal stresses vary as $\eta\,\dot{\gamma}\,f(\boldsymbol{x}/a)$, where $f(\boldsymbol{x})$ is a function of the vector of particle positions $\boldsymbol{x}$. The bulk normal stress is then the average over all possible configurations, weighted by the configuration distribution function $\mathscr{P}(\boldsymbol{x})$. The distribution function $\mathscr{P}(\boldsymbol{x})$, being dimensionless, cannot depend on the magnitude of $\dot{\gamma}$ as there is no other time scale in the problem. However, it depends on the sign of $\dot{\gamma}$, thus resulting in the normal stresses varying as $|\dot{\gamma}|$. This behaviour was demonstrated by Brady & Morris (1997) for dilute suspensions, with particle interactions taken to be pair-wise additive, but the result is valid for arbitrary concentrations. The form of the constitutive relation for the stress for general, non-viscometric, flows is an interesting issue and needs to be addressed in later studies.

Our data show the stress to be largely independent of the particle size, as expected for flow in the Stokes regime. The normal stresses are small at low concentrations, but rise rapidly when ϕ increases. The normal stress coefficients Υ_1 and Υ_2 (negative of the normal stress differences scaled by $|\dot{\gamma}|$) are both positive, in agreement with the findings of Zarraga *et al.* (2000) and Sierou & Brady (2001). Our data for Υ_1 are in good agreement with the results of Stokesian Dynamics simulations of Sierou & Brady and Singh & Nott (2000), but are considerably higher than the experimental data of Zarraga *et al.* The lack of agreement with the latter may be due to their

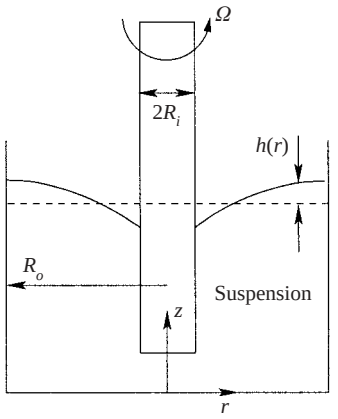

FIGURE 17. The 'rod dipping' effect in Stokesian suspensions.

large measurement error. There is reasonable agreement between our data and that of Zarraga *et al.* for Υ_2, which is found to be significantly larger than Υ_1. However, the simulations of Sierou & Brady show Υ_1 and Υ_2 to be roughly equal.

Sierou & Brady (2001) have speculated that the discrepancy, referred to above, between observations in experiments and simulations arises from frictional contacts between particle in the former, which are forbidden in the latter. While mechanical contact of suspended particles is likely at volume fractions above loose random packing, i.e $\phi \approx 0.5$, they will be far too infrequent at lower concentrations. It is more likely that this discrepancy is due to the effect of repulsive inter-particle forces that are used in the simulations. These short-range interactions play a prominent role in determining the anisotropy of the microstructure, as Sierou & Brady themselves have noted, and their presence in a non-Brownian suspension is in doubt. An attempt to simulate shear of suspensions in the complete absence of non-hydrodynamic forces would prove useful in sorting out this matter (Kumar 2002).

We thank N. Chandrasekhar for his suggestion of using a lock-in amplifier to measure small stresses. Financial support from the Department of Science and Technology, grant III 5(90)/95-ET, is gratefully acknowledged.

Appendix. Perturbation of the free surface due to normal stress differences

Consider a rod of radius R_i rotating with angular velocity Ω in a suspension confined in a cylinder of radius R_o (figure 17). The shear rate at radial position r in the gap is

$$\dot{\gamma} = \frac{-2\Omega R_i^2}{1-\kappa^2}\frac{1}{r^2} = \frac{-A}{r^2},$$

where $\kappa \equiv R_i/R_o$ and $A \equiv (2\Omega R_i^2)/(1-\kappa^2)$.

Neglecting inertia, the radial momentum balance is

$$\frac{1}{r}\frac{\partial}{\partial r}(r\sigma_{rr}) - \frac{\sigma_{\theta\theta}}{r} = 0. \tag{A 1}$$

This can be rearranged and written as

$$\frac{\partial N_2}{\partial r} - \frac{N_1}{r} = -\frac{\partial \sigma_{zz}}{\partial r}. \tag{A 2}$$

The z-momentum balance, which is simply the hydrostatic balance, provides

$$\sigma_{zz} = \sigma^0_{zz} - \rho g h(r), \tag{A 3}$$

where σ^0_{zz} is the hydrostatic head of the unsheared suspension, and $h(r)$ is the deviation of the free surface from the horizontal. Substituting (A 3) in (A 2) yields

$$\frac{\partial N_2}{\partial r} - \frac{N_1}{r} = \rho g \frac{\partial h}{\partial r}. \tag{A 4}$$

Using $N_1 = -\Upsilon_1|\dot{\gamma}|$ and $N_2 = -\Upsilon_2|\dot{\gamma}|$, and integrating (A 4) from R_i to r, yields

$$\rho g\,[h(r) - h\,(R_i)] = -A\left(\Upsilon_2 + \tfrac{1}{2}\Upsilon_1\right)\left[\frac{1}{r^2} - \frac{1}{R_i^2}\right]. \tag{A 5}$$

As the net volume of the suspension remains unchanged, we have

$$\int_{R_i}^{R_o} r h(r)\,\mathrm{d}r = 0. \tag{A 6}$$

From equations (A 5) and (A 6) we obtain

$$\rho g h(R_i) = A\left(\Upsilon_2 + \tfrac{1}{2}\Upsilon_1\right)\left[\frac{\ln(R_o/R_i)^2}{\left(R_o^2 - R_i^2\right)} - \frac{1}{R_i^2}\right]. \tag{A 7}$$

Substituting (A 7) in (A 5), we obtain the extra pressure measured at the outer cylinder due to deflection of the surface,

$$\begin{aligned}\rho g h(R_o) &= \left[1 + \frac{1}{1-\kappa^2}\ln(\kappa^2)\right]\left(N_2 + \tfrac{1}{2}N_1\right)\\ &\equiv -\alpha\left(N_2 + \tfrac{1}{2}N_1\right).\end{aligned} \tag{A 8}$$

For our Couette device, $\kappa = 0.818$, giving $\alpha = 0.214$. This pressure is subtracted from the $\hat{\sigma}_{rr}$ we measure in cylindrical-Couette flow to give the second normal stress difference N_2.

REFERENCES

Acrivos, A., Mauri, R. & Fan, X. 1993 Shear-induced resuspension in a Couette device. *Intl J. Multi-phase Flow* **19**, 797.

Bagnold, R. A. 1954 Experiments on a gravity-free dispersion of large soild spheres in a newtonian fluid under shear. *Proc. R. Soc. Lond.* A **225**, 49.

Barnes, H. A., Hutton, J. F. & Walters, K. 1989 *An Introduction to Rheology*. Elsevier.

Bird, R. B., Armstrong, R. C. & Hassager, O. 1977 *Dynamics of Polymeric Liquids. Volume 1: Fluid Mechanics*. John Wiley and Sons.

Brady, J. F. & Morris, J. F. 1997 Microstructure of strongly sheared suspensions and its impact on rheology and diffusion. *J. Fuild Mech.* **348**, 103.

Chandrasekhar, S. 1961 *Hydrodynamic and Hydromagnetic Stability*. Clarendon.

Cochran, G. W. 1967 *Statistical Methods*. The Iowa State University Press.

Gadala-Maria, F. A. 1979 The rheology of concentrated suspensions. PhD thesis, Stanford University.

Kolli, V. G., Pollauf, E. J. & Gadala-Maria, F. 2002 Transient normal stress response in a concentrated suspension of spherical particles. *J. Rheol.* **46**, 321.

Krishnan, G. P., Beimfohr, S. & Leighton, D. T. 1996 Shear-induced radial segregation in bidisperse suspensions. *J. Fluid Mech.* **321**, 371.

Kumar, P. M. 2002 Effect of hydrodynamics and interparticle forces in sheared suspensions. Master's thesis, Indian Institute of Science.

Leighton, D. T. 1985 The shear-induced migration of particles in concentrated suspensions. PhD thesis, Stanford University.

Leighton, D. T. & Acrivos, A. 1987 The shear-induced migration of particles in concentrated suspensions. *J. Fluid Mech.* **181**, 415.

Luppold, D. S. 1969 *Precision Measurements and Standards.* Addison Wesley.

Macosko, C. W. 1994 *Rheology: Principles, Measurements, and Applications.* VCH Publications.

Morris, J. F. & Boulay, F. 1999 Curvilinear flows of noncolloidal suspensions: the role of normal stresses. *J. Rheol.* **43**, 1213.

Nott, P. R. & Brady, J. F. 1994 Pressure-driven flow of suspensions: Simulation and theory. *J. Fluid Mech.* **275**, 157.

Parsi, F. & Gadala-Maria, F. 1987 Fore-and-aft asymmetry in a concentrated suspension of solid spheres. *J. Rheol.* **31**, 725.

Phung, T. N., Brady, J. F. & Bossis, G. 1996 Stokesian dynamics simulation of brownian suspensions. *J. Fluid Mech.* **313**, 181.

Prasad, D. & Kytoma, H. K. 1995 Particle stress and viscous compaction during shear of dense suspensions. *Intl J. Multiphase Flow* **21**, 775.

Savage, S. B. 1979 Gravity flow of cohensionless granular materials in chutes and channels. *J. Fluid Mech.* **92**, 53.

Sierou, A. & Brady, J. F. 2001 Rheology and microstructure in concentrated non-colloidal suspensions. *J. Rheol.* **46**, 1031.

Singh, A. 2001 Rheology of non-colloidal suspensions. PhD thesis, Indian Institute of Science.

Singh, A. & Nott, P. R. 2000 Normal stresses and microstructure in bounded sheared suspensions via stokesian dynamics simulations. *J. Fluid Mech.* **412**, 279–301.

Zarraga, I. E., Hill, D. A. & Leighton, D. T. 2000 The characterization of the total stress of concentrated suspensions of noncolloidal spheres in Newtonian fluids. *J. Rheol.* **44**, 185.